Int. J. Heat Mass Transfer. Vol. 32, No. 9, pp. 1741–1750, 1989
Printed in Great Britain

0017–9310/89 $3.00 + 0.00

Inverse heat transfer analysis of Bridgman crystal growth

K. TAGHAVI
Department of Mechanical Engineering, University of Kentucky, Lexington, KY 40506, U.S.A.

and

W. M. B. DUVAL
NASA Lewis Research Center, Cleveland, OH 44135, U.S.A.

(*Received* 28 *October* 1988 *and in final form* 20 *February* 1989)

Abstract—The effects of asymmetry in furnace temperature profile and pulling velocity on the crystal interface shape are demonstrated while neglecting the latent heat of solidification. It is seen that the furnace temperature profile may be varied in order to influence the shape of the melt–crystal interface. An exact thermal analysis is then performed on the Bridgman technique by including the latent heat of solidification as a source term. The exact temperature field required for yielding a flat melt–crystal interface is obtained. The earlier observation regarding the influence of furnace temperature profile on the interface shape is confirmed and a criterion for achieving a flat interface is obtained. Various furnace temperature profiles are selected and their corresponding melt–crystal interface results are presented.

1. INTRODUCTION

THE BRIDGMAN technique for crystal growth involves translation of a crucible containing a source material through a multi-zone furnace, which is set at a certain temperature profile [1]. As the ampoule passes through the hot zone and enters the cold zone, the source material solidifies into a crystal state. In practice, it is very difficult to manipulate the melt and crystal temperature profile during the crystal growth. However, in our analysis we consider the case of prescribing a general temperature profile along the axial boundary of the melt and crystal in order to control the melt–crystal interface.

Stress and solute distributions at the melt–crystal interface influence the quality of the grown crystal, e.g. Jordan *et al.* [2], and Chang and Brown [3], respectively. For crystal growth from pure systems where solute distribution can be neglected, control of the macroscopic shape of the interface is necessary in order to grow a crystal with desirable quality for device applications. Minimization of stress and imperfections in the crystal can be achieved by maintaining a planar interface. One way of controlling the interface shape is through the furnace temperature profile. Herein, we investigate the effects of the furnace temperature profile on the melt–crystal interface shape. A criterion is developed for obtaining a planar interface, while taking into account the effect of the latent heat of solidification.

Several works have been performed where the temperature profile and the melt–crystal interface shape were determined; one of the earliest analytical works was performed by Chang and Wilcox [4]. They analyzed an infinitely long ampoule with the boundary condition of heat convection into a constant temperature medium. They included the effect of crystal pulling but ignored the heat source due to the released latent heat of solidification of the melt. Later, Fu and Wilcox [5] solved the same problem numerically and added an insulated region between the hot and the cold regions which was determined to be effective in decreasing the dependence of interface shape to system perturbations.

Huang *et al.* [6] studied the effect of unequal melt and crystal thermal conductivities on the interface shape. They employed a finite element technique to solve for the temperature field, neglecting the released latent heat of solidification. They also studied the effect of anisotropy of the crystal thermal conductivity on the melt–crystal interface shape. The conclusion was that the interface shape is very sensitive to thermal conductivities of the melt and the crystal. Jasinski *et al.* [7, 8] analyzed the temperature field in an approximate manner. In the first paper, the axial dependence of the temperature field is examined while the radial dependence is neglected. In the second paper, the radial heat flux is included by lumping the temperatures of the crucible and the charge into single temperatures. In both of these works, the latent heat of solidification is neglected. Finally, Potts and Wilcox [9] performed experiments on this phenomenon and presented their observation regarding the melt–crystal interface shape. They found that for certain parameter ranges, the interface shape was strongly dependent on the agitation and natural convection in the melt.

NOMENCLATURE

C's	constants of integration used in Appendix B
c_p	specific heat at constant pressure of melt and crystal
d^+	dimensionless furnace temperature as $z \to \infty$, see equation (13)
d^-	dimensionless furnace temperature as $z \to -\infty$, see equation (13)
$F(Z)$	furnace temperature profile
$f(z)$	dimensionless furnace temperature profile, $[F(Z)-T_m]/T_m$
f_0	parameter used to represent constant $f(z)$
$g(z)$	function used to construct furnace temperature profile
g_0	parameter used to represent constant $g(z)$
h_{fs}	latent heat of solidification
i	integer used in summation
J_0	Bessel function of the first kind and zeroth order
J_1	Bessel function of the first kind and first order
k	thermal conductivity of melt and crystal
n	direction normal to solidification front
Pe	Peclet number, $2UR_0/\alpha$
q_l	dimensionless heat flux in melt at solidification front, $[\partial\theta_l/\partial z]$ at $z = z_m$
q_s	dimensionless heat flux in crystal at solidification front, $[\partial\theta_s/\partial z]$ at $z = z_m$
Δq	$q_s - q_l$
R	radial coordinate
R_0	radius of ampoule
r	dimensionless radial coordinate, R/R_0
S	dimensionless parameter, $c_p T_m/h_{fs}$
T	temperature
T_l	temperature of melt
T_m	melting temperature
T_s	temperature of crystal
U	velocity of crystal pulling
Z	coordinate along ampoule
Z_m	location of solidification front
z	dimensionless coordinate along ampoule, Z/R_0
z_m	dimensionless location of solidification front, Z_m/R_0.

Greek symbols

α	thermal diffusivity, $k/\rho c_p$
γ^+	parameter used in furnace temperature profile, equation (13)
γ^-	parameter used in furnace temperature profile, equation (13)
θ	dimensionless temperature, $(T-T_m)/T_m$
θ_l	dimensionless temperature in melt
θ_s	dimensionless temperature in crystal
θ_u	solution to unit step function as a boundary condition at $r = 1$
λ_i	eigenvalues, equation (7)
μ	dimensionless parameter involving crystal pulling velocity, $UR_0(2\alpha) = Pe/4$
ν_i^+	modified eigenvalues, $-\mu+(\mu^2+\lambda_i^2)^{1/2}$
ν_i^-	modified eigenvalues, $\mu+(\mu^2+\lambda_i^2)^{1/2}$
ρ	mass density of melt and crystal.

The purpose of this paper is to investigate the effect of the following parameters or conditions on the melt–crystal interface during crystal growth from the melt by the Bridgman technique.

(1) Combined and individual effects of the asymmetric furnace temperature profile and the crystal pulling.
(2) Heat of solidification.

In this analysis, we initially neglect the release of the latent heat of solidification. This approximation illustrates the effects of furnace temperature profile and crystal pulling on the interface shape. Finally, an exact analysis of the crystallization phenomenon which includes the release of the latent heat of solidification is performed. Because an exact solution seems impossible, we adopt an 'inverse' approach in solving a simple Bridgman crystal growth. While traditionally the furnace temperature profile is given and the melt–crystal interface shape is sought, we proceed to calculate the furnace temperature profile which yields a prescribed interface shape, more specifically a flat melt–crystal interface, hence an 'inverse' solution.

2. APPROXIMATE TREATMENT

In this part of the paper, the latent heat of solidification released by the crystallization phenomenon is assumed to be much smaller than the heat flux at the interface of the melt and the crystal, and that its effect on the crystallization process is negligible. This assumption is reasonable for small pulling velocities. In fact, this approximation becomes exact for a stationary ampoule, i.e. $U = 0$.

2.1. *Analytical model*

The following assumptions are made in the present model.

(1) Melt and crystal regions are much longer than the crystal radius such that these regions may be considered to be infinitely long.
(2) Thermophysical properties of the melt and crystal are equal and independent of temperature.

(3) The coordinate system is attached to the furnace.

(4) The melt solidifies at a constant temperature T_m.

(5) The furnace temperature is circumferentially uniform.

(6) A quasi-steady state is achieved. That is, the temperature profile in the melt or crystal at a fixed axial coordinate is independent of time. As a result, the location and the shape of the melt–crystal interface becomes steady and will stay stationary with respect to the furnace.

(7) The crystal is isotropic.

(8) The ampoule wall is ignored in order to isolate the effects of the furnace temperature profile and the pulling velocity. In the present analysis the temperature boundary condition is chosen to be that of the surface of the melt and crystal, i.e. the inner wall of the ampoule wall. A good approximation for accounting for the ampoule wall is to write a one-dimensional conduction equation relating the temperatures of the inner and outer walls of the ampoule and the thermal resistance of the ampoule wall.

(9) The heat transfer coefficient in the furnace is assumed to be large. As a result, the temperature of the melt and crystal at the inner wall of the ampoule is approximated to be equal to the furnace temperature. A good approximation to treat a finite heat transfer coefficient is to add the convective resistance to the ampoule wall resistance and employ the heat conduction equation similar to that mentioned in assumption (8) above. Hereafter in this paper we refer to our temperature boundary condition as the furnace temperature profile.

(10) No natural convection is present in the melt. It was observed by Chang and Wilcox [4] and Fu and Wilcox [5] that melt natural convection in a vertical Bridgman configuration was negligible for practical crystal growth applications where ampoule radius is small. Further, in microgravity applications, in the absence of any strong gravitational field, natural convection is strongly damped and is negligible.

(11) No thermal radiation effects are present in the melt or crystal.

(12) The effect of impurities or solute concentration on heat transfer are neglected. For the purpose of this study, we are interested in the heat transfer analysis of pure single crystals, e.g. experiments by Singh *et al.* [10] with lead chloride ($PbCl_2$). Various purification processes have been developed to reduce the amount of impurities to insignificant levels necessary for growing bulk crystals. For these situations, therefore, it is not necessary to address the effect of solute concentration or impurities in the melt.

Since the phase change (or the heat of crystallization) is ignored here, and the melt and crystal have equal thermophysical properties, the problem reduces to that of pure conduction in a homogenous medium. The physical model is depicted in Fig. 1. The

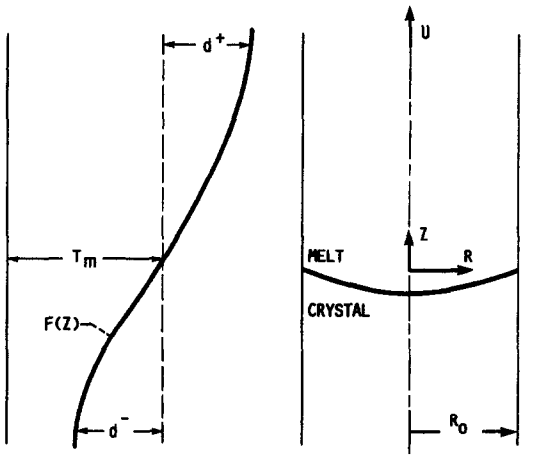

FIG. 1. Physical model depicting the Bridgman technique and the furnace temperature profile.

governing equation for the temperature field in the melt and crystal is

$$U\partial T/\partial Z = \alpha[\partial^2 T/\partial R^2 + (1/R)\partial T/\partial R + \partial^2 T/\partial Z^2] \quad (1)$$

with the boundary conditions

$$T = F(Z) \quad \text{at } R = R_0 \quad (2)$$

$$\partial T/\partial R = 0 \quad \text{at } R = 0. \quad (3)$$

The value of the function F at $Z = 0$ is arbitrarily set to the melting temperature, i.e. $F(0) = T_m$. This forces the melt–crystal interface at the ampoule wall to be located at $Z = 0$. The solution to equation (1) with the boundary conditions (2) and (3) is (from Appendix A)

$$\theta = \sum_{i=1}^{\infty} \frac{J_0(\lambda_i r)}{J_1(\lambda_i)} \frac{\lambda_i}{(\mu^2+\lambda_i^2)^{1/2}} \times \int_0^{\infty} \{e^{-\nu_i^- u} f(z+u) + e^{-\nu_i^+ u} f(z-u)\}\, du \quad (4)$$

where the modified eigenvalues are

$$\nu_i^+ = -\mu + (\mu^2+\lambda_i^2)^{1/2} \quad (5)$$

and

$$\nu_i^- = \mu + (\mu^2+\lambda_i^2)^{1/2} \quad (6)$$

and λ_i is the ith positive root of

$$J_0(\lambda) = 0. \quad (7)$$

In equations (4)–(7), the following set of dimensionless parameters is used:

$$r = R/R_0 \quad (8)$$

$$z = Z/R_0 \quad (9)$$

$$\theta = (T - T_m)/T_m \quad (10)$$

$$\mu = Pe/4 = UR_0/(2\alpha) \quad (11)$$

$$f(z) = [F(Z) - T_m]/T_m. \quad (12)$$

2.2. *Exponential and asymmetric furnace temperature profile*

Here, we assume an asymmetric and exponential temperature profile in the furnace of the form (shown in Fig. 1)

$$f(z) = \begin{cases} d^+(1-e^{-\gamma^+ z}) & z > 0 \\ -d^-(1-e^{\gamma^- z}) & z < 0 \end{cases}. \quad (13)$$

The exponential behavior is chosen for the purpose of illustration and because it yields a simple closed-form solution for the temperature field. Equation (13) represents a continuous temperature profile in the furnace. An additional restriction is made upon the furnace temperature profile: that of a continuous temperature gradient at $z = 0$. This restriction requires that

$$d^+\gamma^+ = d^-\gamma^-. \quad (14)$$

The function $f(z)$ in equation (4) may be replaced by equation (13) to obtain the temperature field

$$\theta = \sum_{i=1}^{\infty} \frac{J_0(\lambda_i r)}{J_1(\lambda_i)} \frac{\lambda_i}{(\mu^2+\lambda_i^2)^{1/2}} \left\{ \frac{d^+}{v_i^-} - \frac{d^+}{v_i^- + \gamma^+} e^{-\gamma^+ z} + \frac{d^+}{v_i^+}(1-e^{-v_i^+ z}) + \frac{d^+}{v_i^+ - \gamma^+}(e^{-v_i^+ z} - e^{-\gamma^+ z}) - \frac{d^-}{v_i^+} e^{-v_i^+ z} + \frac{d^-}{v_i^+ + \gamma^-} e^{-v_i^+ z} \right\} \quad \text{for} \quad z > 0 \quad (15)$$

and

$$\theta = \sum_{i=1}^{\infty} \frac{J_0(\lambda_i r)}{J_1(\lambda_i)} \frac{\lambda_i}{(\mu^2+\lambda_i^2)^{1/2}} \left\{ -\frac{d^-}{v_i^+} + \frac{d^-}{v_i^+ + \gamma^-} e^{\gamma^- z} - \frac{d^-}{v_i^-}(1-e^{v_i^- z}) - \frac{d^-}{v_i^- - \gamma^-}(e^{v_i^- z} - e^{\gamma^- z}) + \frac{d^+}{v_i^-} e^{v_i^- z} - \frac{d^+}{v_i^- + \gamma^+} e^{v_i^- z} \right\} \quad \text{for} \quad z < 0. \quad (16)$$

Equations (15) and (16) represent the temperature field. The crystallization front z_m is defined as the location where the temperature is equal to the crystallization temperature T_m

$$\theta(r, z_m) = 0. \quad (17)$$

Equation (17) together with the temperature field, equations (15) and (16), cannot be solved analytically for the crystallization front. Therefore, these equations are solved numerically to obtain $z_m(r)$.

2.3. *Effect of asymmetry*

Here, the effect of asymmetry in the furnace temperature profile on the melt–crystal interface shape is considered. In order to isolate this effect, the pulling velocity is set to zero. That is, $U = 0$ and therefore $v_i^- = v_i^+ = \lambda_i$. It should be noted that, under this assumption, the approximation of no heat source due to the latent heat of solidification becomes exact. Upon investigating this problem mathematically, it is observed that in the absence of the pulling velocity, the only remaining parameters are γ^- and d^-/d^+. The position of the melt–crystal interface for $\gamma^- = 1$ and various d^-/d^+ is shown in Fig. 2. It is seen that the interface is convex for $d^-/d^+ > 1$ and that the degree of convexity increases with the degree of asymmetry. The interface shape for $d^-/d^+ < 1$, on the other hand, is concave and the degree of concavity increases as d^-/d^+ decreases. It can be shown that $[z_m(r)]_1 = -[z_m(r)]_2$ for $(d^+/d^-)_1 = (d^-/d^+)_2$, where subscripts 1 and 2 represent two different cases. The case of $d^-/d^+ = 1$ denotes a symmetric furnace temperature profile and yields a flat interface.

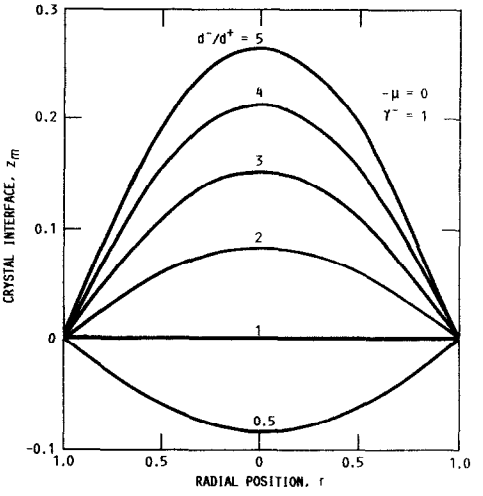

FIG. 2. Location of the melt–crystal interface for various degrees of asymmetry.

2.4. *Effect of crystal pulling*

The effect of crystal pulling on the melt–crystal interface is studied next. To isolate this effect, the furnace temperature profile is assumed to be symmetric, that is, $d^- = d^+ = d$ and $\gamma^- = \gamma^+ = \gamma$. The position of the melt–crystal interface for various pulling velocities is shown in Fig. 3. It is observed that the

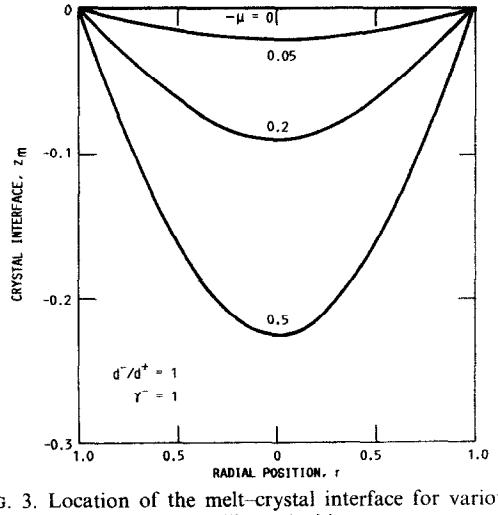

FIG. 3. Location of the melt–crystal interface for various crystal pulling velocities.

interface is concave and that the degree of concavity increases with the pulling velocity. Not shown in the figure are the cases of $\mu > 0$, that is, for upward pulling of the ampoule. For these cases the interface becomes convex with the degree of convexity increasing with the pulling velocity. Again, it may be shown that $[z_m(r)]_1 = -[z_m(r)]_2$ for $\mu_1 = -\mu_2$.

2.5. *Combined effects of asymmetry and crystal pulling*

Figures 2 and 3 indicate opposing effects on the shape of the melt–crystal interface due to asymmetry (for $d^-/d^+ > 1$) and crystal pulling (for $\mu < 0$). This suggests that the effect of one may offset that of the other. To illustrate this, Fig. 4 shows the melt–crystal interface for a particular pulling velocity while the degree of asymmetry in the furnace temperature is changing. As d^-/d^+ increases the interface shape approaches that of a flat surface and the degree of concavity decreases. It is observed that no degree of asymmetry could completely offset the effect of crystal pulling, i.e. resulting in a flat interface. It may be adequate, however, to study the case which results in zero displacement at the center of the ampoule, i.e. $z_m = 0$ at $r = 0$ (a nearly flat interface). This is the subject of the next figure.

Figure 5 shows the degree of asymmetry necessary to maintain zero displacement at the center of the ampoule for each pulling velocity. As expected, higher degrees of asymmetry are necessary for higher crystal pulling velocities.

3. ANALYSIS: INCLUDING THE HEAT OF SOLIDIFICATION

In this part of the work, an analysis which includes the effect of the latent heat of solidification is performed. All of the assumptions listed under Section 2.1 are also valid for this case.

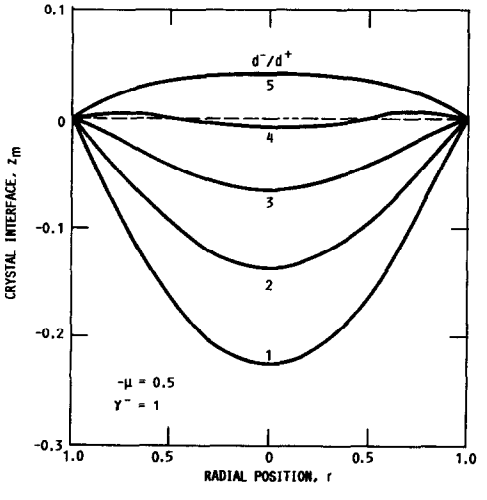

FIG. 4. Location of the melt–crystal interface for various degrees of asymmetry and crystal pulling velocities.

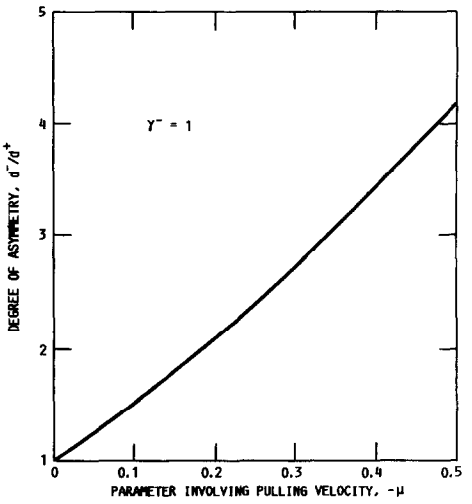

FIG. 5. Degrees of asymmetry necessary to maintain a nearly flat interface as a function of the crystal pulling velocity.

3.1. *Analysis*

In this section the heat of solidification is included in the balance of heat fluxes at the melt–crystal interface, i.e. the complete Stefan-type problem will be treated exactly. This means that an exact interface condition at the crystallization front is adopted. This condition is written as

$$-k[\partial T_s/\partial n]_m = -k[\partial T_l/\partial n]_m + \rho h_{fs} U/[1+(\partial Z_m/\partial R)^2] \quad (18)$$

where n is the direction perpendicular to the interface and the subscript m means that the parameter is evaluated at the crystallization front. The exact analysis of this problem involves elaborate mathematical manipulations and is beyond the scope of this paper. To avoid this, we take advantage of the fact that we are mostly interested in achieving a flat interface between the melt and the crystal. For a flat interface, equation (18) becomes

$$-k[\partial T_s/\partial Z]_{Z_m} = -k[\partial T_l/\partial Z]_{Z_m} + \rho h_{fs} U \quad (19)$$

or, in terms of dimensionless parameters

$$-q_s = -q_l + 2\mu/S \quad (20)$$

where the dimensionless parameters S, q_l, and q_s are defined as

$$S = c_p T_m/h_{fs} \quad (21)$$

$$q_l = [\partial\theta_l/\partial z]_{z=z_m} \quad (22)$$

$$q_s = [\partial\theta_s/\partial z]_{z=z_m}. \quad (23)$$

This problem, just as the classical Stefan problem, is nonlinear and therefore does not have a straightforward solution. To solve this problem, it is divided into two simpler problems and the principle of superposition is used. Figure 6 shows the breakdown of the general problem. The two simpler problems are:

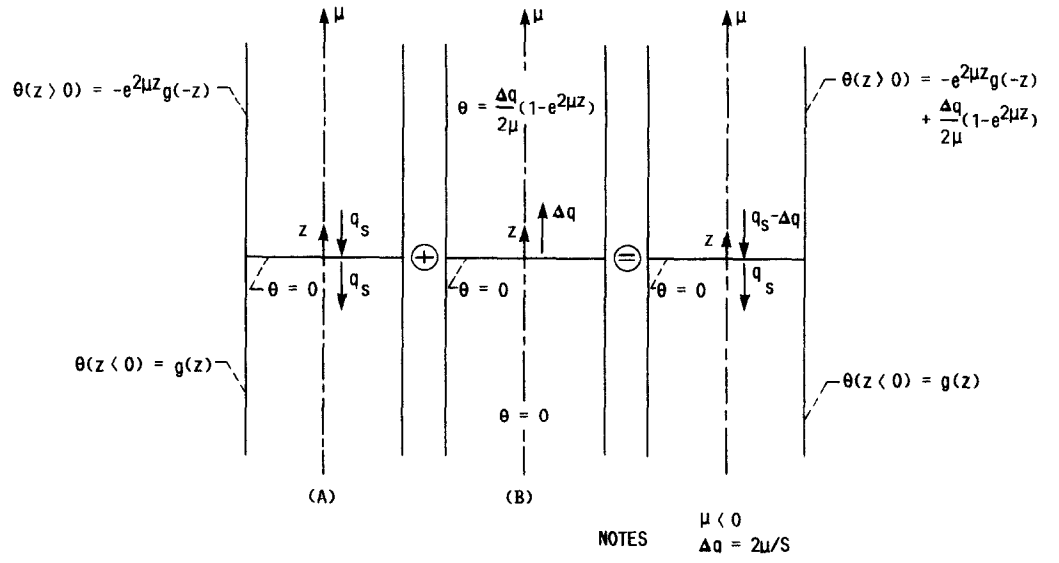

FIG. 6. Dividing the general problem into two simpler problems.

(A) a moving medium with no phase change, with the boundary condition $\theta = g(z)$ at $r = 1$ and the additional requirement that $\theta = 0$ at $z = 0$;

(B) a moving medium with a surface heat source at $z = 0$ and strength of

$$\Delta q = q_s - q_1 = -2\mu/S. \tag{24}$$

The solutions to these two problems are presented in Appendices A and B. The temperature field obtained by superposing the two solutions is

$$\theta_1 = \sum_{i=1}^{\infty} \frac{J_0(\lambda_i r)}{J_1(\lambda_i)} \frac{\lambda_i}{(\mu^2+\lambda_i^2)^{1/2}} \times \int_0^{\infty} \{e^{-v_i^- u} g(z+u) + e^{-v_i^+ u} g(z-u)\}\, du \quad \text{for} \quad z < 0 \tag{25}$$

and

$$\theta_s = \theta_1 + (e^{2\mu z} - 1)/S \quad \text{for } z > 0 \tag{26}$$

where λ_i is given by equation (7), and v_i's are given by equations (5) and (6). To maintain $\theta = 0$ at $z = 0$, it is required (from Appendix A) that

$$g(z) = -e^{2\mu z} g(-z) \quad \text{for } z > 0. \tag{27}$$

Accordingly, the furnace temperature profile may be written as

$$f(z) = -e^{2\mu z} g(-z) + (e^{2\mu z} - 1)/S \quad \text{for } z > 0 \tag{28}$$

$$f(z) = g(z) \quad \text{for } z < 0. \tag{29}$$

The furnace temperature profile described in equations (28) and (29) guarantees a flat melt–crystal interface. There are two degrees of freedom in this problem; μ and $g(z)$. The parameter μ is indicative of how fast the ampoule is being pulled while the function $g(z)$ is indicative of the furnace temperature profile. This function may be chosen to achieve a goal such as uniform heat flux at the interface. In the following sections, three such special cases of furnace temperature profile will be presented.

3.2. *Uniform interface heat flux*

The function $g(z)$ may be chosen to control the dependence of the interface heat flux in the melt or crystal on the radial position r. For example, a constant heat flux at the melt–crystal interface may be desired by the crystal growers. Upon differentiation of the θ relation, equations (25) and (26), with respect to z, evaluating it at $z = 0$, and using equation (27), the dimensionless heat fluxes at the interface are written as

$$q_s = \sum_{i=1}^{\infty} \frac{J_0(\lambda_i r)}{J_1(\lambda_i)} \frac{2\lambda_i v_i^-}{(\mu^2+\lambda_i^2)^{1/2}} \int_0^{\infty} e^{-v_i^- u} g(u)\, du \tag{30}$$

$$q_1 = q_s + 2\mu/S. \tag{31}$$

In order to achieve constant heat flux at the melt–crystal interface, the following property of the Bessel functions is used:

$$\sum_{i=1}^{\infty} \frac{2J_0(\lambda_i r)}{\lambda_i J_1(\lambda_i)} = 1. \tag{32}$$

It is seen that one way the interface heat fluxes in equations (30) and (31) become independent of the radial position is to have

$$\frac{\lambda_i^2[\mu + (\mu^2+\lambda_i^2)^{1/2}]}{(\mu^2+\lambda_i^2)^{1/2}} \int_0^{\infty} e^{-[\mu+(\mu^2+\lambda_i^2)^{1/2}]u} g(u)\, du = q_s \quad \text{for all } i. \tag{33}$$

The above conclusion can also be achieved in a more rigorous manner by expanding the function q_s in terms of Bessel functions of the first kind and zeroth order and equating the coefficients of the similar terms.

Obviously, it is desired that the parameter q_s in equation (33) be independent of the radial position r. Since equation (33) holds for all i, the acceptable solution for $g(z)$ is one that does not depend on i. This equation cannot be satisfied exactly. However, for small μ, i.e. $\mu \ll \lambda_1$, an approximate relationship may be obtained. Assuming that

$$(\mu^2+\lambda_i^2)^{1/2} \simeq \lambda_i+\mu^2/2\lambda_i+\cdots \tag{34}$$

and substituting it into equation (33), and keeping only the leading order terms in μ result in

$$\lambda_i(\lambda_i+\mu)\int_0^\infty e^{-(\mu+\lambda_i)u}\, g(u)\,du \simeq q_s \tag{35}$$

or

$$\int_0^\infty e^{-\lambda_i u}\, e^{-\mu u}\, g(u)\, d(\lambda_i u) \simeq q_s(\lambda_i^{-1}-\mu\lambda_i^{-2}). \tag{36}$$

The acceptable solution is

$$e^{-\mu z}\, g(z) = az+bz^2 \quad \text{for } z>0 \tag{37}$$

while requiring

$$\int_0^\infty e^{-\lambda_i u}\, au\, d(\lambda_i u) = q_s\lambda_i^{-1} \tag{38}$$

and

$$\int_0^\infty e^{-\lambda_i u}\, bu^2\, d(\lambda_i u) = \mu q_s\lambda_2^{-2}. \tag{39}$$

These two integrals can be rewritten in terms of a new variable $v = \lambda_i u$ to obtain

$$\int_0^\infty e^{-v}\, av\, dv = q_s \tag{40}$$

and

$$\int_0^\infty e^{-v}\, bv^2\, dv = \mu q_s. \tag{41}$$

These definite integrals are evaluated and equations (40) and (41) are solved for a and b. The function $g(z)$ can subsequently be written as

$$g(z) = q_s(z+\mu z^2/2)\, e^{\mu z} \quad \text{for } z>0 \tag{42}$$

or, using equation (27)

$$g(-z) = -q_s(z+\mu z^2/2)\, e^{-\mu z} \quad \text{for } z>0. \tag{43}$$

The furnace temperature profile is calculated from equations (28), (29), and (43) as

$$f(z) = q_s(z+\mu z^2/2)\, e^{\mu z}+(e^{2\mu z}-1)/S \quad \text{for } z>0 \tag{44}$$

$$f(z) = -q_s(-z+\mu z^2/2)\, e^{\mu z} \quad \text{for } z<0. \tag{45}$$

There still exists two degrees of freedom; μ and q_s. The solution so far includes a flat crystallization interface and interface heat fluxes that are nearly independent of the radial position. The parameter μ again represents the velocity with which the crystal is pulled. The parameter q_s, while a measure of the interface heat flux in the crystal, is also a measure of the furnace temperature. The larger q_s, the hotter the furnace.

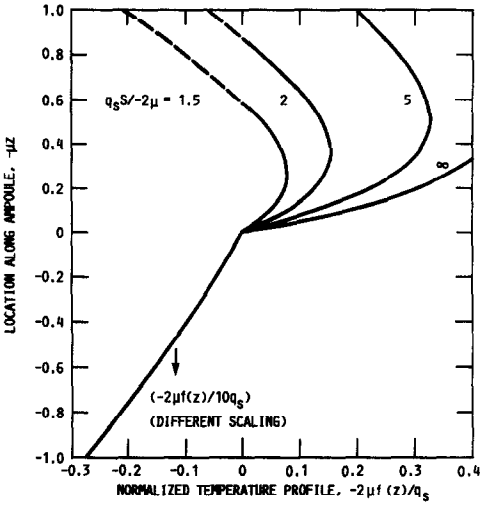

FIG. 7. Furnace temperature profile for uniform heat fluxes at the melt–crystal interface.

Figure 7 shows the furnace temperature profile for various parameters involved in the problem. The vertical axis in this figure is $-\mu z$ (μ is negative). In practical cases $-\mu$ may become as large as 0.1. Considering an ampoule as long as ten times its diameter, it is calculated that $-\mu z$ may become as large as 1. The furnace temperature profile behaves unconventionally and crosses the crystallization temperature (i.e. $f=0$) one time before going to $-1/S$ as $z\to\infty$ (Fig. 7) and becoming very large in magnitude as $z\to-\infty$. But practically, we are interested in the range $1>-\mu z>-1$ which is the range shown in Fig. 7. It is seen that the temperature gradient is discontinuous at $z=0$. This is required to accommodate the latent heat of solidification released at the melt–crystal interface. The figure also shows that for large enough $-\mu z$ the temperature profile crosses the crystallization temperature meaning that the melt material becomes solid again. Obviously this was not considered in the modelling of the problem, and therefore such a conclusion should be avoided by concentrating only on a smaller μz.

Finally, Fig. 7 shows the results for $S\to\infty$ which is equivalent to assuming negligible latent heat of solidification. This curve when compared with the one for the actual S shows the error associated with neglecting the latent heat of solidification.

3.3. *Uniform furnace temperature for $z<0$*

Another plausible candidate for the furnace temperature is a uniform profile. This is desirable due to experimental limitations. Therefore, we assume that

$$g(z) = -g_0 \quad \text{for } z<0. \tag{46}$$

The parameter g_0 is arbitrary and indicates the tem-

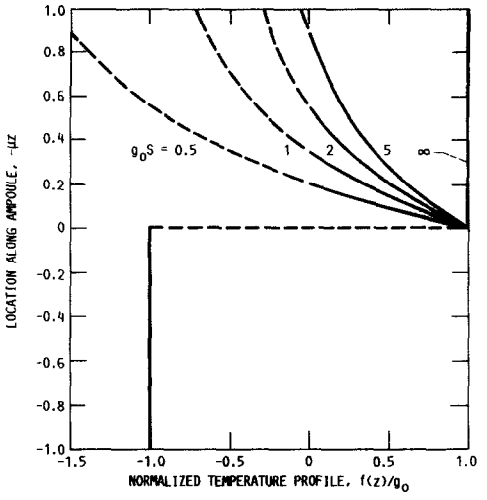

FIG. 8. Furnace temperature profile for uniform temperature in the cold region.

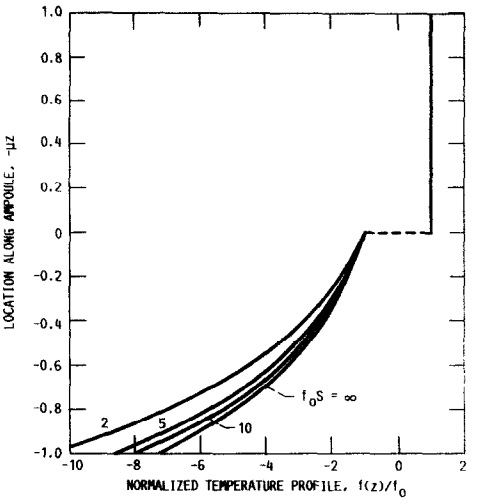

FIG. 9. Furnace temperature profile for uniform temperature in the hot region.

perature level of the furnace. Substituting equation (46) into equations (28) and (29), the furnace temperature profile is obtained as

$$f(z) = g_0 e^{2\mu z} + (e^{2\mu z} - 1)/S \quad \text{for } z > 0 \quad (47)$$

$$f(z) = -g_0 \quad \text{for } z < 0. \quad (48)$$

Note that the discontinuity in the temperature is not in conflict with the earlier requirement that $F(Z = 0) = T_m$, i.e. $f(z = 0) = 0$, if, as in Fourier analysis, $f(0)$ is written as

$$f(0) = \tfrac{1}{2}\{f(0^+) + f(0^-)\} = \tfrac{1}{2}\{g_0 - g_0\} = 0. \quad (49)$$

Figure 8 shows the required furnace temperature profile according to equations (47) and (48). As expected, the temperature is uniform in the lower part of the furnace. At $z = 0$, there is a jump in the temperature. Thereafter, the temperature drops exponentially. This is somewhat uncommon since most furnaces are set so that their temperature increases with z in the upper half of the ampoule. Again, it is observed that far from the interface at some z the temperature of the furnace drops below the melting point which means the melt material should be in the solid state.

Again the special case of $S \to \infty$ is plotted. In this case, the furnace temperature profile in the positive z region is uniform. This compares well with the earlier studies where the furnace consists of uniform hot and cold regions, and the latent heat of solidification is ignored. In those studies the melt–crystal interface obtained was flat.

3.4. *Uniform furnace temperature for $z > 0$*

Finally, the furnace temperature for the upper part may be assumed to be constant as

$$f(z) = f_0 \quad \text{for } z > 0. \quad (50)$$

The function f for $z < 0$ may be obtained by substituting equation (49) in equation (28) and solving for $g(z)$. Then, $f(z)$ is written from equation (29) as

$$f(z) = (1 - e^{2\mu z})/S - f_0 e^{2\mu z} \quad \text{for } z < 0. \quad (51)$$

Again, we have

$$f(0) = \tfrac{1}{2}\{f(0^+) + f(0^-)\} = \tfrac{1}{2}\{f_0 - f_0\} = 0. \quad (52)$$

Figure 9 shows this furnace temperature profile. Similar to the previous case, there is a temperature discontinuity at the crystal interface. The furnace temperature in the cold region becomes colder as it gets further away from the crystal interface which is similar to the conventional furnaces.

3.5. *General comments regarding the furnace temperature profiles*

Figures 7–9 show the required furnace temperature profiles in order to maintain a flat melt–crystal interface and some prescribed furnace characteristic, e.g. constant temperature in the cold region. It should be remembered that there is not complete freedom in choosing the furnace temperature profile. The limitation is indicated in equation (27). This equation, however, only relates the temperature profiles in the hot and cold regions of the furnace (see equations (28) and (29)). Therefore, the selection of $g(z)$ in the positive or negative z region is completely without any restriction. As a result, any desired profile may be prescribed for $g(z)$. Subsequently, equations (28) and (29) may be used to find the corresponding furnace temperature profile.

The furnace temperature profiles depicted in Figs. 7–9 are mathematical results of the desired characteristics, e.g. constant temperature in the cold region of the furnace. These profiles may not be readily attainable in a laboratory setup. For example, the profiles in Figs. 8 and 9 require a temperature discontinuity at $z = 0$. Although such a profile is not practical, a furnace approaching this profile may be

designed by using effective insulation around the location of $z = 0$. Therefore, these temperature profiles are best utilized if looked upon as ideal goals that the real furnaces should approach.

Finally it should be noted that the common value of the parameter $-\mu$ corresponding to the Bridgman setups is about 0.05. Therefore, the practical range of interest in the $-\mu z$ coordinate is (assuming an aspect ratio of 10 for the ampoule)

$$-0.5 < -\mu z < 0.5. \tag{53}$$

This limited range will eliminate some anomalies in the obtained temperature profiles. For example, the hot region of Fig. 7 indicates a temperature profile that first increases and then decreases, eventually resulting in melt resolidification (i.e. $\theta < 0$). According to equation (53), the profile in Fig. 7 does not show the above mentioned anomaly within the concerned range and may be viewed to be reasonable.

4. SUMMARY AND CONCLUDING REMARKS

A simplified Bridgman technique is analyzed. The effects of crucible wall, solute concentration, melt convection, and variable thermophysical properties are ignored. Neglecting the heat source due to the latent heat of solidification, it was shown that the melt–crystal interface shape is influenced by the furnace temperature profile and the pulling velocity. It was observed that asymmetry in the furnace temperature profile and pulling velocity may have opposite effects on the interface shape and that these effects may never completely counterbalance each other and yield a flat interface. However, some results were obtained relating the required degree of asymmetry for each pulling velocity in order to achieve a nearly flat interface.

Later the effect of latent heat of solidification was included. The resulting temperature field was obtained for the case of a flat interface. This exact analysis also provided a criterion for the furnace temperature profile in order to obtain a flat interface. Thereafter, various furnace temperature profiles were adopted and the corresponding results were presented. It was seen that most of the calculated furnace temperature profiles were unlike the common profiles where the furnace temperature monotonically increases from the cold to the hot regions.

Acknowledgements—This work was performed during the first author's appointment as a Summer Faculty Fellow at the NASA Lewis Research Center. The authors thank Prof. G. Young for many helpful discussions.

REFERENCES

1. B. R. Pamplin, *Crystal Growth* (2nd Edn), p. 7. Pergamon Press, Oxford (1980).
2. A. S. Jordan, A. R. Von Neida and R. Caruso, The theory and practice of dislocation reduction in GaAs and InP, *J. Crystal Growth* **70**, 555–573 (1984).
3. C. J. Chang and R. A. Brown, Radial segregation induced by natural convection and melt/solid interface shape in vertical Bridgman growth, *J. Crystal Growth* **63**, 343–364 (1983).
4. C. C. Chang and W. R. Wilcox, Control of interface shape in the vertical Bridgman–Stockbarger technique, *J. Crystal Growth* **21**, 135–140 (1974).
5. T.-W. Fu and W. R. Wilcox, Influence of insulation on stability of interface and position in the vertical Bridgman–Stockbarger technique, *J. Crystal Growth* **48**, 416–424 (1980).
6. C. E. Huang, D. Elwell and R. S. Feigelson, Influence of thermal conductivity on interface shape during Bridgman growth, *J. Crystal Growth* **64**, 441–447 (1983).
7. T. Jasinski, W. M. Rohsenow and A. F. Witt, Heat transfer analysis of the Bridgman–Stockbarger configuration for crystal growth: analytical treatment of the axial temperature profile, *J. Crystal Growth* **61**, 339–354 (1983).
8. T. Jasinski, A. F. Witt and W. M. Rohsenow, Heat transfer analysis of the Bridgman–Stockbarger configuration for crystal growth: analytical treatment of radial temperature variations, *J. Crystal Growth* **67**, 173–184 (1984).
9. H. Potts and W. R. Wilcox, Thermal fields in the Bridgman–Stockbarger technique, *J. Crystal Growth* **73**, 350–358 (1985).
10. N. B. Singh, W. M. B. Duval and B. N. Rosenthal, Characterization of directionally solidified lead chloride, *J. Crystal Growth* **89**, 80–85 (1988).
11. H. S. Carslaw and J. C. Jaeger, *Conduction of Heat in Solids* (2nd Edn). Oxford University Press, Oxford (1959).

APPENDIX A. A MOVING MEDIUM WITH $\theta = g(z)$ AT $r = 1$

The schematic of this problem is shown in Fig. 6(A). In order to solve this problem, we start with the solution to a unity step function boundary condition and then apply the principle of superposition to obtain the solution to a more general problem. The unit step function boundary condition is written as

$$\theta = 1 \quad \text{at} \quad r = 1 \quad \text{and} \quad z > 0 \tag{A1}$$

$$\theta = 0 \quad \text{at} \quad r = 1 \quad \text{and} \quad z < 0. \tag{A2}$$

The solution to this problem may be obtained from Carslaw and Jaeger [11] and with a little manipulation is written as

$$\theta_u = 1 - \sum_{i=1}^{\infty} \frac{\nu_i^- J_0(\lambda_i r)}{\lambda_i J_1(\lambda_i)(\mu^2 + \lambda_i^2)^{1/2}} e^{-\nu_i^+ z} \quad \text{for } z > 0 \tag{A3}$$

$$\theta_u = \sum_{i=1}^{\infty} \frac{\nu_i^+ J_0(\lambda_i r)}{\lambda_i J_1(\lambda_i)(\mu^2 + \lambda_i^2)^{1/2}} e^{\nu_i^- z} \quad \text{for } z < 0 \tag{A4}$$

where the subscript u is used to denote that the solution is for a unit step function boundary condition. The eigenvalues λ_i and the modified eigenvalues ν_i^+ and ν_i^- are defined as

$$J_0(\lambda_i) = 0 \tag{A5}$$

$$\nu_i^+ = -\mu + (\mu^2 + \lambda_i^2)^{1/2} \tag{A6}$$

$$\nu_i^- = \mu + (\mu^2 + \lambda_i^2)^{1/2}. \tag{A7}$$

Now, the principle of superposition may be used to obtain the general solution as

$$\theta = g(-\infty)\theta_u(z; -\infty) + \int_{-\infty}^{\infty} (dg/d\zeta)\theta_u(z; \zeta)\, d\zeta \tag{A8}$$

where $\theta_u(z; \zeta)$ is the solution to a unit step function located at $z = \zeta$. Equation (A8) may be integrated by parts to obtain

$$\theta = -\int_{-\infty}^{\infty} g(\zeta)[\partial\theta_u(z; \zeta)/\partial\zeta]\, d\zeta. \tag{A9}$$

In obtaining equation (A9), the following properties of the

solution to a unit step function, equations (A3) and (A4), have been used:

$$\lim_{\zeta\to-\infty}\theta_u(z;\zeta)=1 \tag{A10}$$

and

$$\lim_{\zeta\to\infty}\theta_u(z;\zeta)=0. \tag{A11}$$

Equation (A9) can now be evaluated by replacing θ_u from equations (A3) and (A4) to obtain

$$\theta=\sum_{i=1}^{\infty}\frac{J_0(\lambda_i r)}{J_1(\lambda_i)}\frac{\lambda_i}{(\mu^2+\lambda_i^2)^{1/2}}\int_0^{\infty}\{e^{-\nu_i^- u}g(z+u)+e^{-\nu_i^+ u}g(z-u)\}\,du. \tag{A12}$$

In addition to the boundary conditions imposed so far, this problem requires that $\theta(r,0)=0$. It may be concluded from equation (A12), when evaluated at $z=0$, that the only possible solution is to have the integrand identically equal to zero. This reduces to a restriction on $g(z)$ as

$$g(z)=-e^{2\mu z}g(-z). \tag{A13}$$

APPENDIX B. A MOVING MEDIUM WITH SURFACE HEAT SOURCE AT $z=0$

The schematic of this problem is shown in Fig. 6(B). Since the heat source is uniformly distributed on a flat surface and there is no boundary condition imposed at $r=1$, the problem reduces to that of a one-dimensional case. The governing equation is written as

$$d^2\theta/dz^2=2\mu\,d\theta/dz \tag{B1}$$

with

$$\theta=0 \quad \text{at } z=0 \tag{B2}$$

and

$$-\left[\frac{d\theta}{dz}\right]_{z=0^+}+\left[\frac{d\theta}{dz}\right]_{z=0^-}=\Delta q \tag{B3}$$

where Δq is the strength of the source at the plane $z=0$. The general solution to equation (B1) is

$$\theta=C_1e^{2\mu z}+C_2. \tag{B4}$$

Taking into consideration that $\mu<0$, the acceptable solution is

$$\theta=C_1^+e^{2\mu z}+C_2^+ \quad \text{for } z>0 \tag{B5}$$

$$\theta=C_2^- \quad \text{for } z<0. \tag{B6}$$

Applying boundary condition (B2) and interface condition (B3) yields

$$C_2^-=C_1^++C_2^+=0 \tag{B7}$$

and

$$C_1^+=-\Delta q/2\mu. \tag{B8}$$

The solution can now be written as

$$\theta=-(\Delta q/2\mu)(e^{2\mu z}-1) \quad \text{for } z>0 \tag{B9}$$

$$\theta=0 \quad \text{for } z<0. \tag{B10}$$

The heat source Δq is related to the velocity of the moving medium as

$$\Delta q=-2\mu/S. \tag{B11}$$

Substituting equation (B11) into equations (B9) and (B10) yields

$$\theta=(e^{2\mu z}-1)/S \quad \text{for } z>0 \tag{B12}$$

$$\theta=0 \quad \text{for } z<0. \tag{B13}$$

ANALYSE DU TRANSFERT THERMIQUE INVERSE DE LA CROISSANCE DU CRISTAL SELON BRIDGMAN

Résumé—Les effets de la dissymétrie du profil de température d'un four et de la vitesse de déformation de l'interface du cristal sont démontrés en négligeant la chaleur latente de solidification. On voit que le profil de température du four peut être modifié de façon à changer la forme de l'interface du cristal. Une analyse thermique exacte est conduite sur la technique de Bridgman par introduction de la chaleur latente de solidification comme un terme source. On obtient le champ de température exact nécessaire pour former un interface plat bain–cristal. L'observation antérieure concernant l'influence du profil de température du four sur la forme de l'interface est confirmée et on obtient un critère pour un interface plan. Plusieurs profils de température du four sont sélectionnés et les résultats correspondant à l'interface sont présentés.

INVERSE ANALYSE DES WÄRMETRANSPORTS BEIM BRIDGMAN-KRISTALLWACHSTUM

Zusammenfassung—Der Einfluß einer asymmetrischen Temperaturverteilung im Ofen und die Auswirkungen der Ziehgeschwindigkeit auf die wachsende Kristalloberfläche werden dargestellt, wobei die zur Verfestigung benötigte latente Wärme zunächst vernachlässigt wird. Es zeigt sich, daß mit einer Variation des Temperaturprofils im Ofen die Form der Grenzfläche zwischen Schmelze und erstarrendem Kristall beeinflußt werden kann. Mit Hilfe der Bridgman-Technik wird der Vorgang thermisch genau untersucht, wobei auch die Kristallisationswärme als Wärmequelle berücksichtigt wird. Es ergibt sich das exakte Temperaturfeld, welches aufgeprägt werden muß, um eine flache Kristalloberfläche zu erzeugen. Eine frühere Untersuchung zum Einfluß der Ofentemperatur wird bestätigt, und ein Kriterium für eine flache Oberfläche wird angegeben. Es werden verschiedene Temperaturprofile des Ofens ausgewählt und die dabei entstehenden Kristallformen vorgestellt.

АНАЛИЗ ОБРАТНОГО ТЕПЛОПЕРЕНОСА ПРИ ВЫРАЩИВАНИИ КРИСТАЛЛОВ ПО МЕТОДУ БРИДЖМЕНА

Аннотация—В пренебрежении скрытой теплотой затвердевания показано влияние асимметрии температурного профиля печи и скорости вытягивания кристалла на форму его межфазной границы. Выявлено, что для оказания влияния на форму поверхности раздела между расплавом и кристаллом можно варьировать температурный профиль печи. Проведен точный тепловой анализ метода Бриджмена с учетом скрытой теплоты затвердевания в качестве источникового члена. Получено точное температурное поле, требуемое для получения плоской поверхности раздела между расплавом и кристаллом. Подтвержден сделанный ранее вывод относительно влияния температурного профиля печи на форму межфазной границы, а также получен критерий для плоской границы. Сделан подбор различных температурных профилей печи и представлены соответствующие результаты для поверхности раздела между расплавои и кристаллом.